851

Temperature Field and Cooling Rate of Laser Cladding with Wire Feeding

Jae-Do Kim*, Yun Peng

Department of Mechanical Engineering, Inha University

Temperature field and cooling rate are important parameters to influence the properties of clad layer and the heat affected zone. In this paper the temperature field and cooling rate of laser cladding are studied by a two-dimensional time-dependent finite element model. Experiment has been carried out by Nd:YAG laser cladding with wire feeding. Research results indicate that at the beginning of cladding, the width and depth of melt pool increase with cladding time. The cooling rate is related to position, cladding time, cladding speed, and preheating temperature. The temperature near melt pool changes rapidly while the temperature far from melt pool changes slowly. With the increase of cladding time, cooling rate decreases. The further the distance from the melt pool, the lower the temperature and the slower the cooling rate. The faster the cladding speed, the faster the cooling rate. The higher the preheating temperature, the slower the cooling rate. The FEM results coincide well with the experiment results.

Key Words : Laser Cladding, Wire Feeding, Temperature Field, Cooling Rate, FEM

1. Introduction

Laser is a high energy density power and has the potential of producing high quality clad layer. Laser cladding has been used for production of parts of composite materials and repair of worn parts. Integral metallurgical bond and low dilution of clad layer are required for laser cladding. Some papers contributed experiment researches in properties of clad layer and dilution of melt pool. (Koshy, 1985; Ramous, 1989; Denney and Duhamel, 1998; Damborene et al., 1993; Fouquet et al., 1994; Tosto et al., 1994; Yellup, 1995; Atamert, and Bhadeshia, 1989; Hirose et al., 1992; Liu et al., 1994; Uenishi and Kobayashi, 1993)

Cooling rate is an important parameter to influence the properties of clad layer and heat affected zone (HAZ). Fast cooling of melt pool metal will

---
* Corresponding Author,
  E-mail : Kimjaedo@inha.ac.kr
  TEL : +82-32-860-7316; +82-32-868-1716
  Department of Mechanical Engineering, Inha University, 253, Yong Hyun-dong, Inchon 402-751, Korea.
  (Manuscript **Received** February 3, 2000; **Revised** May 23, 2000)

result in non-equilibrium microstructures. Mohanty et al. used a laser-assisted visualization technique to monitor the solidification behavior at the tail of a molten pool created by high energy laser beam. The influence of flow instability on the resulting microstructure was analyzed. (Mohanty and Mazumder, 1998) In HAZ, cooling rate influences the staying time of metal at high temperature and results in different degree of austenite grain growth. Cooling rate also decides the microstructure of HAZ. So cooling rate can result in different mechanical properties.

Several mathematical models were presented to simulate the mechanism of laser processing. Kar et al. and Mazumder et al. proposed mathematical models for determining the composition of metastable alloy of extended solid solution. Both the pool and the substrate were taken to be one-dimensional. The distribution of solute atoms in the cladding pool was obtained using diffusion theory with non-equilibrium partitioning of solute at the solid-liquid interface. (Kar and Mazumder, 1988; Kar and Mazumder, 1989; Mazumder and Kar, 1987) Chan et al. developed a two-dimensional model for convective heat

transfer and surface tension driven fluid flow. The model described the transient behavior of the heat transfer process of a stationary band source. Semi-quantitative understanding of scanning is obtained by a coordinate transformation. (Chan et al., 1984) Yang et al. studied the dilution and convection patterns in laser cladding layer. (Yang et al., 1992) Hoadley et al. developed a two-dimensional finite element model for laser cladding by powder injection. It took into account the melting of the powder in the liquid pool and the surface shape and position. (Hoadley and Rappaz, 1992) Frenk et al. deduced the solidification conditions from a two dimensional heat flux model and the phase diagram parameters to discuss the experiment results. (Frenk et al., 1993) Agrawal et al. used a model for extended solid solution to construct a non-equilibrium phase diagram and discussed the influence of initial mean pool temperature, laser power and speed of workpiece on solute composition. (Agrawal et al., 1993)

Some analytical solutions were also proposed. Bamberger et al. assumed one-dimensional heat flow into the workpiece and deduced mathematical formulas for estimating the operating parameters of laser cladding. (Bamberger et al., 1998) Picasso et al. deduced mathematical formulas for the 3-D analytical solution of melt pool of laser cladding. Beam velocity and powder feed rate could also be computed for a given laser power, beam width, and geometry of the powder-injection jet. (Picasso et al., 1994) Powell et al. developed a theoretical model to analyze thermal cycling and dilution during laser cladding process. (Powell et al., 1988)

Hoadley's model (Hoadley and Rappaz, 1992) simulated the longitudinal section of clad track. The heat loss out of the longitudinal plane was neglected. This simplification applies when the width of the base metal is almost as wide as the laser beam. On the other hand, quasi-steady temperature field, and constant and very low dilution ($<1\%$) are assumed in his model. So, this situation is suitable for special situation and doesn't represent a general laser cladding process.

For a moving heat source projecting on a base

metal, the overall heat flow is three dimensional. But near the end of melt pool, heat flow is essentially in the transverse cross section because the temperature gradient in the transverse cross section is much larger than that in the longitudinal section. (David and Vitek, 1989) So, the heat flow outside the cross section may be neglected near this part. In this paper, the model is based on the analysis of heat flow in the end part of the melt pool and the heat flow is assumed to be in the transverse cross section. Time-dependent finite element analysis is conducted. Temperature fields and cooling rates after different cladding times are calculated. The effects of cladding speed and preheating temperature on cooling rate and temperature field are predicted. Experiment of laser cladding with wire feeding has been carried out. The influences of cladding time and cladding speed on the shape of clad layer and the grain size of HAZ are studied.

2. FEM Analysis

2.1 Physical model

Figure 1 shows the physical model. Laser beam with uniformly distributed power strikes on a rectangular area of base metal and moves relative to it. Cladding material is filled into the melt pool. The height of clad layer depends on the feeding speed of cladding material and its surface tension. If the feeding speed is adapted to the width of clad layer, the height of clad layer can be kept constant. Here, a constant height of clad
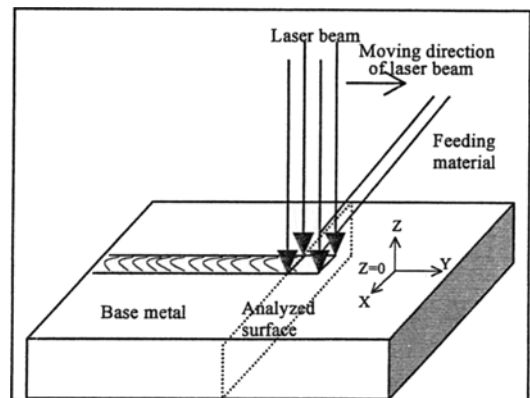

Fig. 1   Schematic diagram of the model

layer is adopted. The shape of the clad layer depends on the physical properties of cladding material and base metal. Here it is assumed that the upper surface of clad layer is a plane and the parts between the upper surface of the clad layer and the base metal surface are in the shape of quarter of circle. The point where the clad layer connects with the base metal is assumed to be at the surface point of base metal where the melting line locates.

The basic assumptions for the model are:

(1) The thermal conductivity, specific heat and density are independent of temperature. In melt pool, these parameters are proportional to the volume fractions of cladding material and base metal.

(2) Latent heat effects are neglected. In the small volume of melt pool, latent heat of fusion is compensated by the latent heat of solidification.

(3) Liquid convection in the melt pool is neglected.

(4) The overall heat conduction is 3-dimensional. In the end part of melt pool, heat conduction is assumed to be in the transverse sections perpendicular to the cladding direction near the end part of melt pool.

During laser cladding, the reference frame is set to attach to the laser beam. At a certain time, the reference frame is set to attach to the base metal. Cooling time begins when the reference frame just departs from the laser beam.

2.2 Formulation

The general finite element equation is

$$M\dot{T}+KT=F \qquad (1)$$

Let t_n denote a typical time in the response so that $t_{n+1}=t_n+\Delta t$, where $n=0, 1, 2, \cdots, N$. Introduce a parameter θ such that $t_\theta=t_n+\theta \cdot \Delta t$, where $0 \leq \theta \leq 1$. M: Heat capacity matrix , K: Conductivity matrix, F: Nodal force vector . We can write the above energy equation at t_θ:

$$M\dot{T}_\theta+KT_\theta=F(t\theta) \qquad (2)$$

Introduce the approximations:

$$\dot{T}_\theta=\frac{T_{n+1}-T_n}{\Delta t} \qquad (3)$$

Table 1 Physical properties of cladding material and base metal

	Inconel 600	Inconel 690
k(W/m·k)	23	37.7
h(W/m²·k)	100	100
T_m(k)	1643	1555
ρ(kg/m³)	8420	7950
c(J/kg·k)	580	836

$$T_\theta=(1-\theta) \cdot T_n+\theta \cdot T_{n+1} \qquad (4)$$
$$F(t\theta)=(1-\theta) \cdot F(t_n)+\theta \cdot F(t_{n+1}) \qquad (5)$$

We have:

$$\bar{K} \cdot T_{n+1}=\bar{F}_{n+1} \qquad (6)$$

where

$$\bar{K}=\theta \cdot K+\frac{1}{\Delta t}M \qquad (7)$$

$$\bar{F}_{n+1}=\left[-(1-\theta) \cdot K+\frac{1}{\Delta t}M\right] \cdot$$
$$T_n+(1-\theta) \cdot F_n+\theta \cdot F_{n+1} \qquad (8)$$

The FEM computation has been done by C language programming. Table 1 shows the physical properties used for the computation.

2.3 FEM results and discussion

2.3.1 Adaptive mesh

Because the shape of melt pool changes during cladding, it is necessary to adapt the mesh to the instant shapes of melt pool, so that the mesh can represent the changing shape of the modeled object during cladding. To realize it, an assumed melting line is preset. After one round computation a computed melting line is obtained. By comparing the preset melting line with the computed values, a new melting line is reset and the mesh is adapted to them. Then the computation is repeated. These steps repeat until the difference between computed melting line and the former set melting line is smaller than 0.0001 mm. The method of mesh adaptation can be expressed as:

$$x_{n+1}=x_n+\omega \cdot (x_m-x_n) \qquad (9)$$
$$y_{n+1}=y_n+\omega \cdot (y_m-y_n) \quad (0<\omega<1) \quad (10)$$

where (x_m, y_m) are computed values.
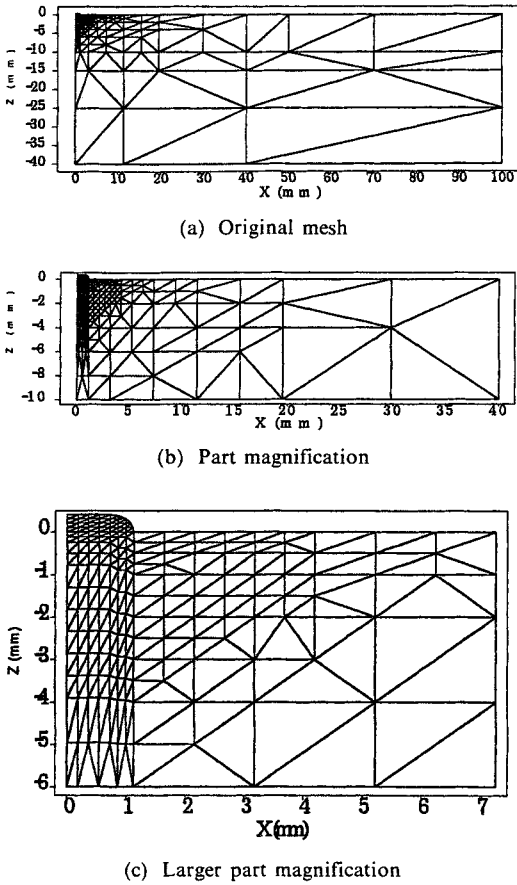
Figure 2 shows the original mesh. Because of

(a) Original mesh

(b) Part magnification

(c) Larger part magnification

Fig. 2   Original mesh

(a) Cladding time 4.8s

(b) Cladding time 7.2s

(c) Cladding time 14s

Fig. 3   Meshes and thermal fields at different clad-
ding times

the symmetry of temperature field in the cross
section, only half of the section is meshed. A mesh
composed of 432 triangle elements is adopted for
the computation. During computation the mesh
adapts its shape and position according to the
melt pool shape automatically. Figure 3 shows
the adapted mesh and the distribution of tempera-
ture fields at different cladding time.

2.3.2   Temperature field and cooling rate

It is assumed that the laser beam shoots perpen-
dicularly on the base metal and distributes uni-
formly in a rectangle area of 3mm × 3mm. The
absorbed power density f is calculated by the
following formulation:

$$f = \eta \times P / [W \times (L + v)] \qquad (11)$$

where L is the spot length (in the cladding direc-
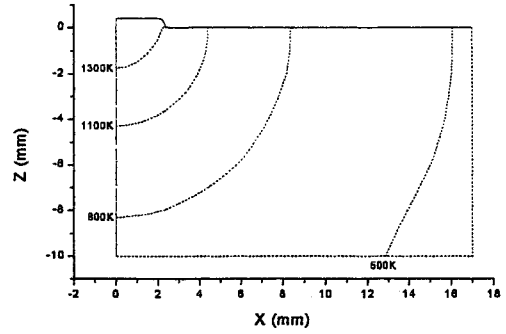tion), W is the spot width (transverse to the

cladding direction), and (is the absorptivity of
laser power P, which is dependent on the mate-
rials and the surface condition of base metal and
feeding materials, such as surface finishing, oxy-
gen content, and the flow rate of assisting gas
(Liu et al., 1994; Ono et al., 1987). Here, it is
assumed that 60% of the laser power is absorbed
by the base metal and cladding material (Li and
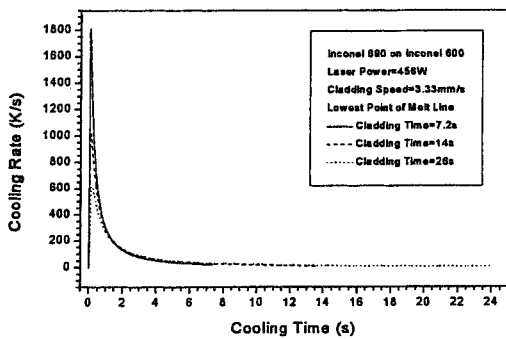Mazumder, 1984). The size of cross section of the
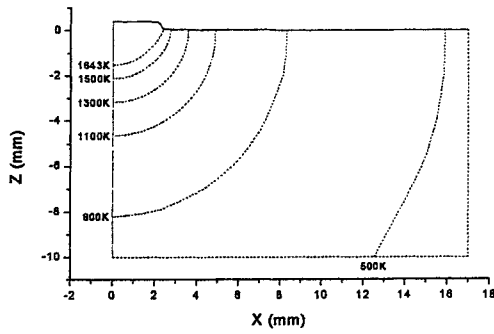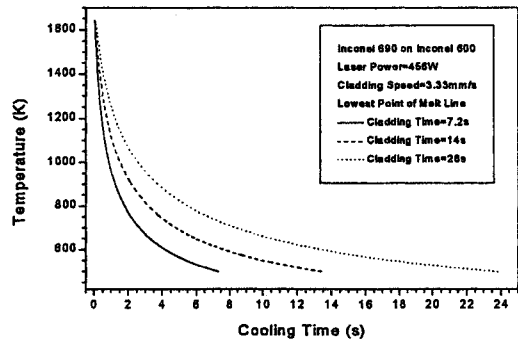
(a) Thermal field at 38s of cladding time   (b) Thermal field after 1.06s cooling

Fig. 4 Thermal fields at 38s of cladding time and after 1.06s cooling

(a) Cooling rates during cooling   (b) Temperatures during cooling

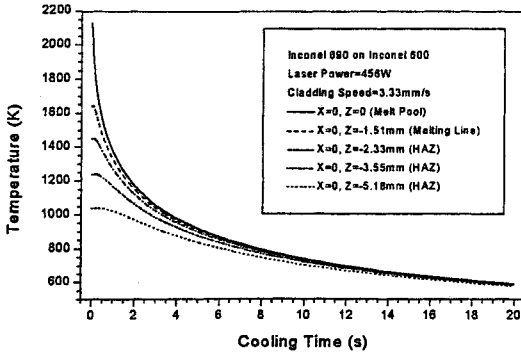**Fig. 5** Temperatures and cooling rates during cooling after different cladding times

base metal perpendicular to the cladding direction is a rectangle of 200mm × 40mm. The cladding material is Inconel 690 and the base metal is Inconel 600. The ambient temperature is adopted to be 298°K.

Figure 3 and Figure 5 (a) illustrate the temperature fields at different cladding times, while the laser power is 456 W. The iso-temperature line of 1643°K is the melting line. After 1.06 s of cooling time, the temperature of original 1643°K iso-temperature line becomes near 1300°K, but at the distance further than 5 mm from the center of melt pool, the temperature shows little change. These figures indicate that during cladding, the temperature near the melt pool increases, resulting in the increase of depth and width of melt pool, as shown in Fig. 4.

Figure 5 (a) and (b) show the temperature field after 38 s of cladding time, and the temperature field of this section after cooling of 1.06 s, respectively. They indicate that towards the melt pool

the temperature gradient increases rapidly. During cooling the temperature near the melt pool changes faster. Another words, the temperature of high temperature zone (near melt pool) decreases faster during cooling. In the area far from the melt pool temperature changes slowly because (1) the temperature gradient is small, and (2) the heat conducted away is partly compensated by the heat conducted into the area.

Figure 6 shows the variations of cooling rate and temperature during cooling after different cladding times. Before quasi-static state is reached, the heat input into the melt pool is faster than heat conducted away from the area. After longer cladding time, the cooling rate is slower than that after shorter cladding time. For increase of cladding time from 7. 2 s to 14 s, the highest cooling rate at about 0.5 s of cool time decreases from 1800°K/s to 1000°K/s. For increase of cladding time from 14 s to 26 s, the highest cooling rate decreases from 1000°K/s to 650°K/s. These
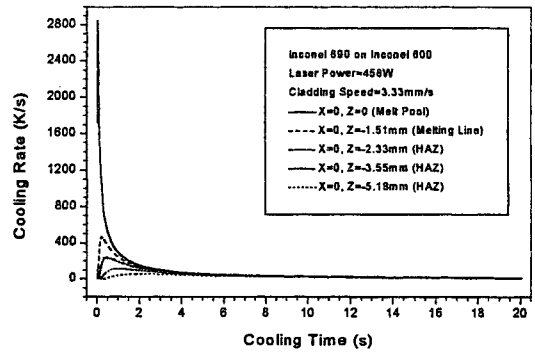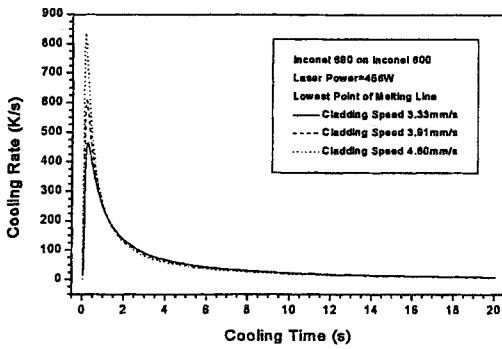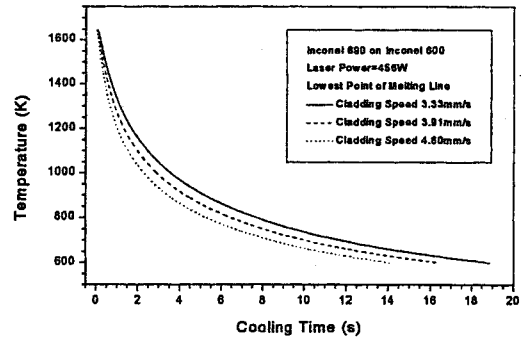
(a) Temperatures during cooling   (b) Cooling rates during cooling

Fig. 6   Temperatures and cooling rates during cooling at different positions

(a) Cooling rates during cooling   (b) Temperatures during cooling

Fig. 7   The effect of cladding speed on temperature and cooling rate

results indicate that with the increase of cladding time the metal will stay at high temperature for longer time.

Figure 7 shows the variations of temperature and cooling rate during cooling for different points. Before cooling the temperature at the center of melt pool reaches to 2100°K. At the melting line 1.51 mm away from the center of melt pool it is 1650°K. At 2.33 mm away from the center of melt pool it is 1450°K. At 3.55 mm away from the center of melt pool it is 1250°K. At 5.18 mm away from the center of melt pool it is 1050 °K. During cooling, from the center of melt pool to 5.18 mm away from it, more time is needed to reach to the highest temperature. From the center of melt pool to 1.51 mm, 2.33 mm, 3.55 mm and 5.18 mm distance away from it, the highest cooling rate decreases from 2850°K/s to 450°K/s, 250°K/s, 100°K/s, and 50°K/s, respectively. These results indicate that with the increase of

distance from melt pool, there is a temperature gradient. The temperature decreases and its cooling rate becomes slower away from the melt pool.

Figure 8 shows the effects of cladding speed on the variation of cooling rate and temperature. For 456 W of laser power as the cladding speed increases from 3.33 mm/s to 3.91 mm/s and to 4. 60 mm/s, the cooling rate increases from 460°K/ s to 610°K/s and to 840°K/s.

Figure 9 shows the effects of preheating temperature on cooling rate and temperature. Given a laser power of 380W, the cooling rate decreases from 840°K/s to 600°K/s and to 425°K/s as the preheating temperature increases from 298°K to 398°K and to 498°K.

The cooling rate influences the microstructure, which in turn determines the mechanical properties of the material. So the prediction of cooling rate may be useful when predicting mechanical
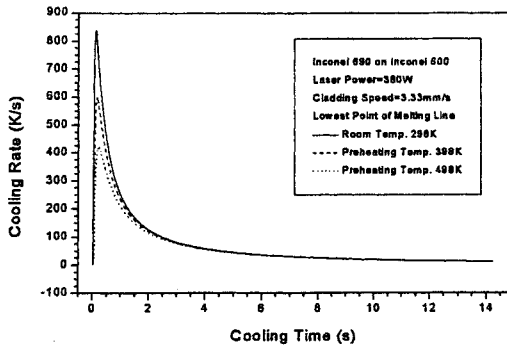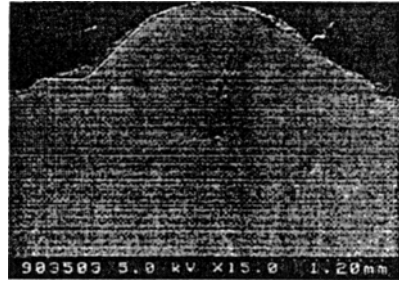
(a) Cooling rates during cooling
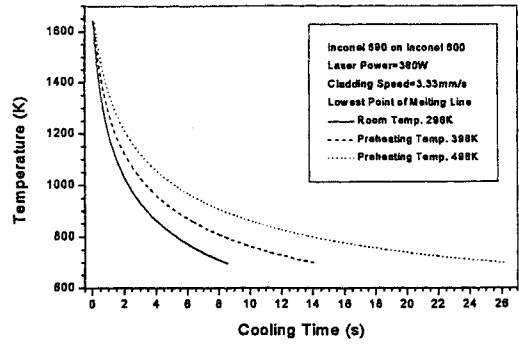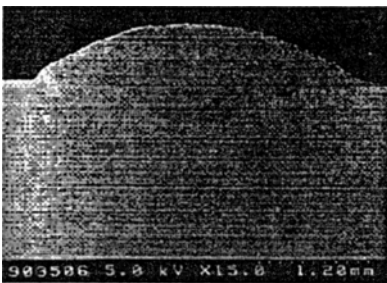

(b) Temperatures during cooling

Fig. 8 The effect of preheating temperature on cooling rate

(a) Cladding speed=1.5mm/s, 5mm away
from the beginning

(b) Cladding speed=1.5mm/s, 25mm
away from the beginning

(c) Cladding speed=2mm/s, 25mm away
from the beginning

(d) Cladding speed=2.5mm/s, 25mm
away from the beginning

Fig. 9 Cross sections of clad layers

properties of the microstructure.

A non-uniform temperature field induces thermal stress. The study of temperature field of laser cladding may be helpful when predicting residual stress of the structure. The cooling rate determines the microstructure of melt pool and HAZ metal. The study of cooling rate may enable to predicting the service properties of the structure.

3. Experiment Results and Discussion

Laser cladding with wire feeding has been done by Nd: YAG laser. The parameters used for the experiment are: beam mode: TEM_{00}, frequency: 20 Hz, peak power: 5.5 kW, average power: 220 W. The optical fiber is used to conduct the laser beam. Beam diameter is 2.5 mm. Argon is used as shielding gas to protect the melt metal and cool

the nozzle of laser beam. Inconel 600 wire of 0.2 mm diameter is used as the feeding wire. Inconel 600 plate is used as the base metal. Wire feeding speed is kept constant with the speed of 93 mm/s while cladding speed is changed. After the laser power shoots on the base metal for 3 seconds, the workpiece begins to move and the wire begins to feed.

Figure 10 (a) and (b) show two cross sections of a clad layer which are 5 mm and 25 mm distance away from the beginning of clad layer, respectively. It is seen that the depth and dilution of clad layer at 25 mm distance from the beginning are much larger than those at 5 mm distance away from the beginning. An observation of the cross section of clad layer also indicates that the width of clad layer is different from the width of melt pool in the base metal. With the increase of distance from the beginning of clad layer, the width of melt pool in the base metal increases significantly, but the width of clad layer shows only a little change.

The changes of width and depth of melt pool are because of the accumulation of heat near melt pool during cladding. The very slow change of width of clad layer results from the constant wire feeding volume per unit distance because the shape of clad layer is not changed significantly.
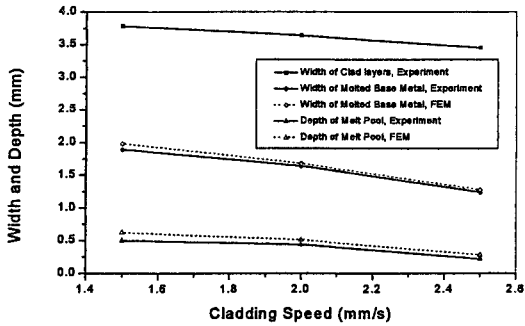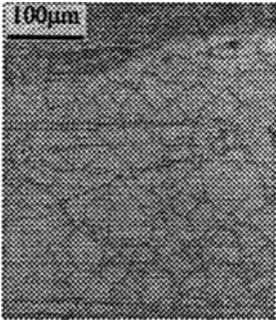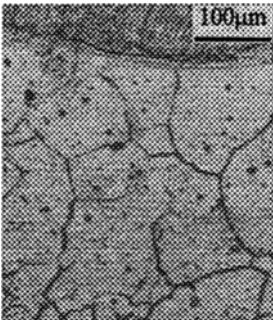

Fig. 10   Width and depth of melt pool at different cladding speed at the cross section 25mm away from the beginning

(a)   Cladding speed=2.5mm/s, 25mm distance from the beginning

(b)   Cladding speed=1.5mm/s, 25mm distance from the beginning

(c)   Cladding speed=1mm/s, 25mm distance from the beginning

(d)   Cladding speed=1mm/s, 5mm distance from the beginning

Fig. 11   Microstructure in the heat-affected zone

During cladding, part of the melted metal flows beyond the width of melt pool in the base metal and bond with the base metal during cooling.

Figure 10 (b), (c), and (d) show that with the increase of cladding speed, the width (in base metal) and depth of melt pool decrease. The decrease of width and depth of melt pool results from the decrease of input line energy with the increase of cladding speed.

Figure 11 (a), (b), and (c) show that with the decrease of cladding speed, the grain sizes of HAZ become larger. Figure 11 (c) and (d) show that for longer cladding time the grain sizes will become larger. They indicate that lower cladding speed results in the HAZ metal staying longer time at high temperature.

Concluding the above discussion, it is indicated that the FEM results coincide well with the experiment results.

4. Conclusions

(1) By the time-dependent FEM modeling with adaptive mesh, the temperature field and cooling rate can be analyzed. The FEM results coincide well with the experiment results.

(2) During laser cladding, heat accumulates near melt pool before quasi-static state is reached, resulting in the increase of depth and width of melt pool during cladding.

(3) Cooling rate is related to cladding time, distance from melt pool, cladding speed, and preheating temperature. The temperature at melting line changes from 1643°K to 1300°K after 1.06 s of cooling time, while the temperature 5 mm away from the melt pool shows little change. With the increase of cladding time from 7.2 s to 14 s and to 26 s, the highest cooling rate decreases from 1800°K/s to 1000°K/s and to 650°K/s, respectively. From the center of melt pool to 1.51 mm, 2.33 mm, 3.55 mm and 5.18 mm distance away from it, the highest cooling rate decreases from 2850°K/s to 450°K/s, 250°K/s, 100°K/s, and 50°K/s, respectively. As the cladding speed increases from 3.33 mm/s to 3.91 mm/s and to 4.60 mm/s at a laser power of 456W, the cooling rate increases from 460°K/s to 610°K/s and to

840°K/s. As the preheating temperature increases from 298°K to 398°K and to 498°K at a laser power of 380W, the cooling rate decreases from 840°K/s to 600°K/s and to 425°K/s.

Acknowledgement

References

Agrawal, G., Kar, A. and Mazumder, J., 1993, *Scripta Metallurgic et Materialia 28*, (11), pp. 1453~1458.

Atamert, S., and Bhadeshia, H. K. D. H., 1989, *Metall. Trans.* A 20A, (6), pp. 1037~1054.

Bamberger, M., Kaplan, W. D., Medres, B. 1998, *J. Laser Appl.*, Vol. 10, No. 1, pp. 29~33.

Chan, C., Mazumder, J. and Chen, M. M., 1984, *Metall. Trans.* A, Vol. 15A, pp. 2175~2184.

Damborene, J. J., Vazquez, A. J., Lopez, V. *Processing of Advanced Materials* Vol. 3, No. 2, pp. 107~113, ISSN: 0960-314X.

David, S. A. and Vitek, J. M., 1989, *Int. Mater. Rev.*, vol. 34, pp. 213~45.

Denney, P. E. and Duhamel, R., 1998, *Industrial Laser Review*, November pp. 19~21.

Fouquet, F., Sallamand, P., Millet, J. P. 1994, *J. Phys.* (France) IV4, (C4), pp. 89~92.

Frenk, A., Henchoz, N., and Kurz, W., *Zeitschrift Fur Metallkunde* 84, (12), pp. 886~892, Dec. 1993. ISSN: 0044~3093.

Hirose, A., Kohno, W., Nomura, D. 1992, *Tetsu~To~Hagane* (Journal of the Iron and Steel Institute of Japan) Vol. 78, No. 10, pp. 1585~1592.

Hoadley, A. F. A. and Rappaz, M., 1992, *Metall. Trans.* B, Vol. 23B, pp. 631~642.

Kar, A. and Mazumder, J., 1988, *Acta Metall.* Vol. 36, No. 3, pp. 701~712.

Kar, A. and Mazumder, J., 1989, *Metall. Trans.* A, Vol. 20A, pp. 363~371.

Koshy, P., 1985, Conference: Applications of

High Power Lasers, Los Angeles, California, USA, 22~23 Jan. 1985; Publ: SPIE, The International Society for Optical Engineering, P. O. Box 10, Bellingham, Washington 98227~0010, USA, pp. 80~85.

Li, L. J. and Mazumder J., 1984, *Laser Processing of Materials* (edited by Mukherjee, K. and Mazumder, J.), pp. 35~50. Proc. Metal. Soc. AIME, Los Angeles, Calif.

Liu, Y., Mazumder, J. and Shibata, K., 1994, *Metall. Mater. Trans. B 25B*, No. 5, pp. 749 ~759.

Mazumder, J. and Kar, A., 1987, *J. Met.* Vol. 39, No. 2, pp. 18~23.

Mohanty, P. S., and Mazumder, J., 1998, *Metall. Mater. Trans.* B, Vol. 29B, pp. 1269 ~1279.

Ono, M., Kosuge, S., Nakada, K. 1987, Conference: LAMP'87: Laser Advanced Materials Process~Science and Applications, Osaka, Japan, 21 ~23 May 1987; Publ: High Temperature Society of Japan, c/o Welding Research Institute of Osaka University, 11~1 Mihogaoka, Ibaraki, Osaka 567, Japan, pp. 395~400.

Picasso, M., Marsden, C. F., Wagniere, J. D. 1994, *Metall. Mater*. Trans. B, Vol. 25B, pp. 281 ~291.

Powell, J., Henry, P. S. and Steen, W. M., 1988, *Surf. Eng*. Vol. 4, No. 2, pp. 141~149.

Ramous, E., 1989, Conference: Surface Engineering With High Energy Beams: Science and Technology, Lisbon, Portugal, 25-27 Sept. 1989; Publ: CEMUL, Av. Rovisco Pais, 1096 Lisboa Codex, Portugal, pp. 425~433.

Tosto, S., Pierdominici, F. and Bianco, M., 1994, *J. Mater. Sci*. Vol. 29, No. 2, pp. 504~509.

Uenishi K. and Kobayashi, K. F., 1993, *Kei Kinzoku Yosetsu* (Journal of Light Metal Welding and Construction) Vol. 31, No. 4, pp. 1~5.

Yang, X., Zheng, T., Zhang, N. 1992. *Acta Metallurgica Sinica (China)* Vol. 28, No. 2, pp. B84~B88, Feb. ISSN: 0412~1961.

Yellup, J. M., 1995, *Surf. Coat. Technol*. Vol. 71, No. 2, pp. 121~128, ISSN: 0257-8972.